NeuroImage 196 (2019) 248–260

Contents lists available at ScienceDirect

NeuroImage

journal homepage: www.elsevier.com/locate/neuroimage

Determinants of structural segregation and patterning in the human cortex

Frithjof Kruggel [a,*], Ana Solodkin [b]

[a] Department of Biomedical Engineering, University of California, Irvine, USA
[b] Department of Anatomy & Neurobiology, University of California, Irvine, USA

ARTICLE INFO

Keywords:
Human cortex
Structural variability
Sulcal roots
Cortical communities

ABSTRACT

This study aimed at uncovering mechanisms that govern the spatio-temporal patterning of the human cortex and its structural variability, and drawing links between fetal brain development and variability in adult brains. A data-driven analytic approach based on structural MR images revealed the following findings: (1) The cortical surface can be subdivided into 13 independent regions ("communities") based on macroscopic features. (2) Thirty centers of low inter-subject variability were found in major sulci on the cortical surface. Their variability showed a strong positive correlation with the known time points at which they appear in fetal development. Centers forming early induce a higher inter-subject regularity in a larger local vicinity, while those forming later result in smaller regions of higher variability. (3) The layout of sulcal and gyral patterns within a community is governed typically by two centers. Depending on the relative variability of each center, communities can be classified into structural sub-types. (4) Sub-types across ipsi-lateral communities are independent, but associated with the sub-type of the same community on the contra-lateral side. Results shown here integrate well with current knowledge about macroscopic, microscopic, and genetic determinants of brain development.

1. Introduction

The quest to understand the relationship between brain and behavior has typically included an intermediate step in the form of brain parcellation. Indeed, the individual variability of macro-structural features of the cerebral cortex has puzzled neuro-anatomists for two centuries (Gratiolet, 1854; Eberstaller, 1890; Cunningham, 1892; Duvernoy, 1991), who, from visual observation, developed a common ontology (Swanson, 2015). Considerable training is required for a human observer to recognize cortical structures. Difficulties arise because even major sulci and gyri show a remarkable structural variability within and between subjects (Ono et al., 1990). Secondary features may be prevalent in some individuals only, and there is an abundance of literature describing detailed regional variation (e.g., Tomaiuolo et al., 1999; Chiavaras and Petrides, 2000; Kringelbach and Rolls, 2004; Germann et al., 2005; Kahnt et al., 2012). However, the definition of regions under study and criteria for sub-type classification are often phenomenological and ad-hoc. An over-arching "theory of cortical variability" trying to assess and interpret the relationship between common and individual features of the human cortex is currently missing.

Existing brain atlas schemes used in anatomical and functional MRI studies (e.g., Tzourio-Mazoyer et al., 2002; Desikan et al., 2006; Oishi et al., 2008; Glasser et al., 2016) are based on the implicit assumption that all brains can be sufficiently represented as a common mean, without assessing the validity of this assumption. The positional error incurred from mapping an individual brain into a normative space is generally well above the current resolution limit of modern neuroimaging methods. No current approach allows referencing the individual variability found on the cortical surface at the imaging level of detail, limiting the advance of knowledge about individual determinants in translational research and clinical practice.

In the present work, rather than focusing on commonalities, we aimed to elucidate mechanisms that govern cortical variability. We applied a data-driven, quantitative approach for assessing individual cortical variability, based on the analysis of anatomical MR brain imaging data acquired in a large cohort of healthy adults. Without including anatomical knowledge, our unbiased approach used machine-learning methods to reveal processes that segregate cortical space while allowing individual variations. As a first step, we introduce background and terminology used in this study:

Sulcal roots: Neuroanatomical studies of fetal development have established locations and time points at which sulci first appear on the cortical surface (Cunningham, 1892; Chi et al., 1977; Nishikuni and Ribas, 2012). Regis et al. (1995, 2005) introduced the term "sulcal roots"

* Corresponding author. 202 Rockwell Engineering Center, University of California, Irvine, CA, 92697-2755, USA.
E-mail address: fkruggel@uci.edu (F. Kruggel).

https://doi.org/10.1016/j.neuroimage.2019.04.031
Received 6 February 2019; Received in revised form 21 March 2019; Accepted 8 April 2019
Available online 14 April 2019

for these initial locations, and was one of the first to suggest the analysis of structural variations in terms of their number and relative configuration. More recently, analyses of in utero MRI data sets (Dubois et al. 2008, 2014; Hu et al., 2011; Clouchoux et al., 2012; Habas et al., 2012) have provided hints that sulcal roots are retained as the locally deepest points within sulci ("pits"). Studies in infants (Meng et al., 2014) and adults (Lohmann et al., 2008; Im et al., 2010; le Guen et al., 2018a) have shown that pits can serve as anatomical landmarks that have a low inter-subject variability (for a recent review, refer to: Im and Grant, 2018).

Basins: We introduced the concept of sulcal basins as a richer representation of cortical features than points (Yang and Kruggel, 2008; Kruggel, 2018). A basin corresponds to a cortical patch that is centered around a locally deepest point and includes the neighboring sulcal area up to the gyral crowns (Fig. 1). Basins are automatically segmented on a surface representing the gray/white matter (GM/WM) interface, using as criteria, geodesic depth and surface curvature. In this way, basins provide a complete segmentation of the cortical surface.

Variability: In our previous publication (Kruggel, 2018), we demonstrated how basin segmentations can be used to quantify inter-individual structural variability. In this context, cortical variability is a point-wise measure that corresponds to a weighted sum of the probabilities of finding specific basins at that location across a group of subjects. If the same basin is found at a specific location across all subjects, the variability is zero. Higher values indicate a higher structural variability (Fig. 2). We demonstrated that neighboring basins cluster into *cortical communities*: basins overlap within a community but not across communities when compared across subjects. Thirteen communities were derived by automated clustering (Fig. 3).

In this work, we assess biological mechanisms that govern cortical variability. We will demonstrate that: (1) The structural pattern within the 13 communities described before (Kruggel, 2018) is governed by 30 centers of low inter-subject variability (CLV) located in major sulci. (2) Their variability shows a strong positive correlation with the known time points at which they appear in fetal development. Deep, low variable centers are formed early in development. (3) The layout of sulcal and gyral patterns within a community is governed by typically two centers. Deep, low variable centers induce a higher regularity in a larger local vicinity. Depending on the relative variability of each center, communities can be classified into structural sub-types. (4) Sub-types across ipsi-lateral communities are independent, but associated with the sub-type of the same community on the contra-lateral side. Community sub-types offer a "pattern library" that is sufficiently large to represent individual variability.

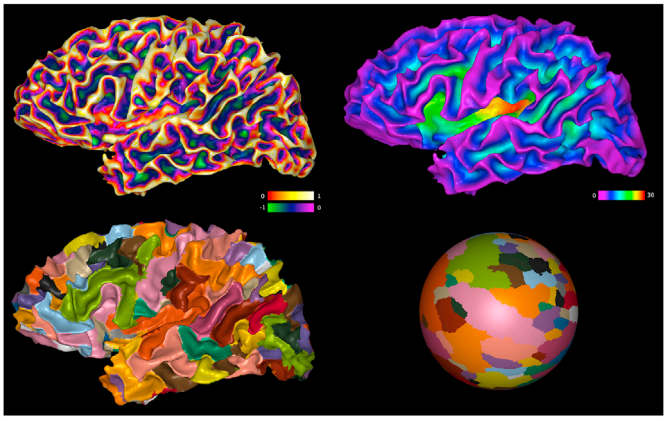

Fig. 1. Processing stages for basin segmentation: Surface shape index (top left, dimensionless units), geodesic depth (top right, in mm), basin segmentation (below left, arbitrary color labels), and aligned spherical map (below right, arbitrary color labels).

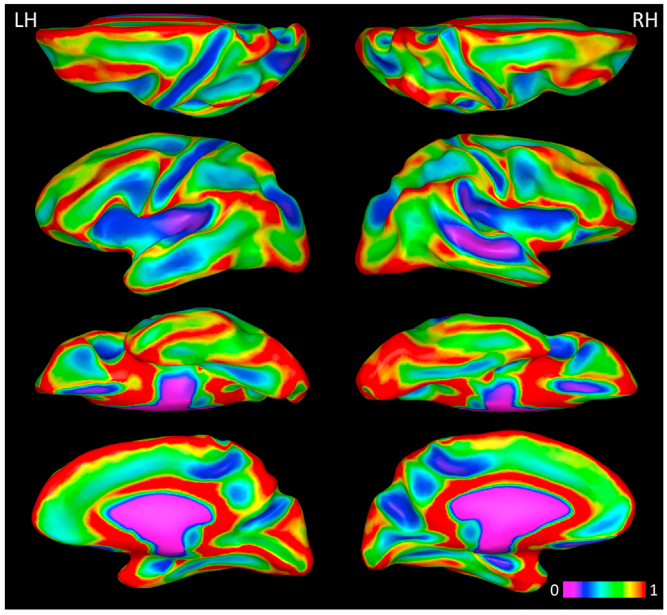

Fig. 2. Overall mapping of variability onto example "inflated" left and right brain hemispheres. Focal regions of a low variability (in magenta) are surrounded by highly variable "rims" (in red). There is a correspondence between variability and geodesic depth: regions of low variability are found in deep cortical folds.

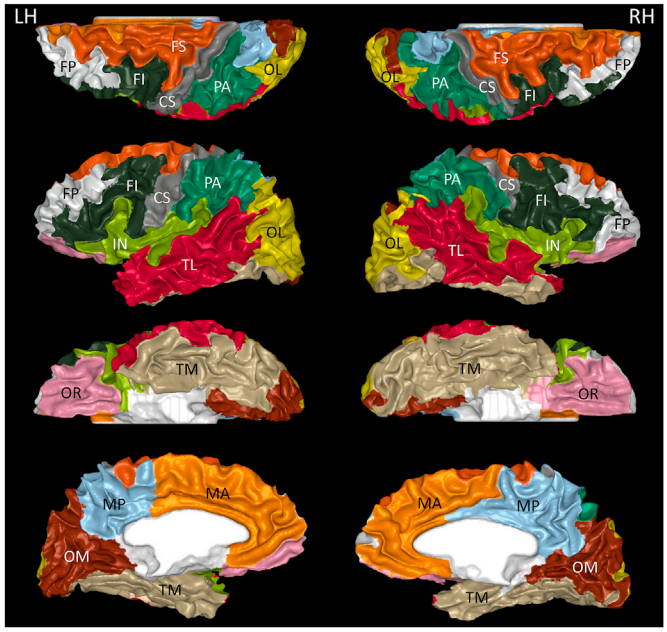

Fig. 3. Mapping of 13 cortical communities onto example left and right brain hemispheres: fronto-superior (FS, dark orange); fronto-polar (FP, white); fronto-inferior (FI, black); central sulcus (CS, gray); parietal (PA, dark green); insula (IN, light green); temporo-lateral (TL, red); occipito-lateral (OL, yellow); orbital (OR, pink); temporo-medial (TM, light brown); occipito-medial (OM, brown); medial-anterior (MA, light orange); medial-posterior (MP, light blue).

2. Material and methods

2.1. Subjects and imaging data

This work included imaging data of the 1113 subjects in the "1200 Subjects Release" of the Human Connectome Project released in March

2017. The cohort consisted of 606 females and 507 males in the age range of 22–37 years (mean: 28.7 years). T1-and T2-weighted structural MR images were used in this study. For detailed acquisition information, refer to the release document (Human Connectome Project, 2017).

2.2. Segmentation of cortical features

The analytical procedures described in this section were extended from our previous work (Yang and Kruggel, 2008; Kruggel, 2018), and we included only relevant detail here.

Generation of hemispheric surfaces: Native T1-and T2-weighted structural images were co-registered, corrected for intensity inhomogeneities, and the intracranial space was extracted. This space was classified into four compartments, roughly corresponding to GM, WM, cerebro-spinal fluid (CSF) and connective tissue. The inner cavities of the WM segmentation (e.g., inner ventricles, basal ganglia) were filled to form a binary object with genus zero. The cerebellum and brain stem were clipped 15 mm below the AC-PC plane, and split into hemispheres at the mid-sagittal plane. A triangulated surface was computed from this object, and optimally adapted to the GM/WM interface. These meshes retained the individual dimensions of the acquired images (0.7 mm vertex distance, about 230.000 vertices, 0.35 mm^2 Voronoi area per vertex). Cortical thickness (Osechinskiy and Kruggel, 2012) and myelin ratio (Glasser and van Essen, 2011) were determined at each vertex location, using the intensity-corrected T1-and T2-weighted images.

Segmentation of cortical basins: Surface curvature was computed from the hemispheric mesh, represented by the shape index (Fig. 1, p. 4). Geodesic depth was determined in image space, using a constrained distance transform on the sulcal compartment and interpolated at vertex positions (Fig. 1, p. 4). Finally, basins were segmented by a watershed-region growing process guided by surface curvature and geodesic depth. Each basin received a unique label stored at each vertex (Fig. 1, p. 4). Regions that were clipped at the mid-sagittal plane and the brain stem were excluded from the process. This procedure yielded 100–140 basins per hemisphere. Basins implicitly encode surface properties: their borders correspond to shallow cortical ridges, and centers to deep sulcal folds.

Inter-subject alignment: To compare data across individuals, each hemispheric mesh was unfolded to a unit sphere while minimizing angle and area distortion (Kruggel, 2008). The overall correspondence between individual spherical meshes was maximized by finding a rotation that optimizes the normalized mutual information of the vertex-wise basin labels with an arbitrarily chosen reference. Finally, basin labels were re-sampled on an icosahedral mesh matching the spatial resolution of the original data (ico7, 163842 vertices; Fig. 1, p. 4). Likewise, geodesic depth, curvature, cortical thickness, and myelin ratio were re-sampled at each vertex location. This process led to a spatial normalization across individuals: Each vertex was considered as homologue between individuals. Technically, data for each hemisphere were stored as a 3D matrix of the 1113 subjects by 163842 vertices by 5 features, along with the spherical mesh that represented vertex positions and neighborhood relationships.

2.3. Cortical variability and communities

This section contains a condensed version of the methods published in (Kruggel, 2018). Please, refer for details to this publication.

Variability map: If all brains had identical surface features, basin labels at each vertex would also be identical. Using the basin segmentation of an example brain as a reference, we computed a basin variability map as follows: For a reference sphere S_r with M basin labels and an object sphere S_o with N basin labels, we collected an $M \times N$ matrix $O(m,n)$ of label correspondences. Nonzero entries in row m of this matrix correspond to the number of vertices that overlap between basin m in the reference and basins n on the object mesh. The row-wise maximum denotes the basin on S_o that best corresponds to basins m on the reference. This map of homologue basins was used to relabel basins of S_o in terms of S_r. For a given reference, this process was repeated for all subject meshes. Next, we determined the frequencies of labels at each vertex, and ranked them by decreasing values, denoting the top rank as zero. Their rank-weighted sum was used as our vertex-wise variability metric V. The variability is zero for a one-to-one match m to n, while any other overlapping basins increase the metric by the amount of overlap, weighted by the rank. All vertices of basin m received the variability score V_m corresponding to this basin. Using one subject as a reference, averaging the 1112 pair-wise variability maps resulted in an individual variability map. Averaging all 1113 individual maps led to the overall variability map (Fig. 2, p. 5).

Community map: Neighboring basins were clustered as communities in terms of their mutual overlap. For a chosen reference mesh S_r, labels on a subject mesh S_o were re-labeled as described above, to find a matrix O of dimensions $M \times M$ that contains the occurrence of label correspondences. Elements on the diagonal of this matrix contain the number of homologue labels between the reference and the subject mesh, and off-diagonal elements the number of vertices in non-homologue basin pairs. Community building was performed by a graph-based algorithm (Fortunato, 2008). Initially, this graph contains an unconnected set of M nodes that represent the basins of the reference mesh. For each off-diagonal non-zero matrix element, an edge was added to the graph, and the edge weight updated by the amount of overlap ("connection strength"). Given the same reference S_r, this process was repeated for all subject meshes S_o, accumulating edge weights in the reference graph. Communities were formed as subsets of nodes that maximized their common connectivity while minimizing their cross-community connectivity. The final number of communities emerged from the heuristic optimization process (Campigotto et al., 2014). Each subject mesh was selected once as the reference, resulting in 1113 maps of community clusters. To integrate all individual community maps, a variability map was computed from the community labeling, as described above. Regions of low variability were occupied by the same community in all subjects, bordered by small rims of high variability where neighboring communities "compete" for space. A watershed-region growing procedure was used to segment this variability map into 13 communities for each hemisphere (Fig. 3, p. 6). This set of communities is considered as the structural core that is common to all the brains in our cohort. Community-wise variability maps (as shown in Fig. 4, and 8-10) were computed by determining the basins that comprise a specific community in each subject, and computing a variability map as described above. Maps were thresholded such that at least 50% of all subjects contributed to a given vertex position.

2.4. Community sub-types

The arrangement of basins within a community may differ across groups of subjects. We examined for community sub-types using the following steps:

Pair-wise similarity: A subject pair was selected, and vertex-wise basins labels within a specified community were compiled in a contingency matrix. If patterns are identical, this matrix has non-zero entries only on the diagonal. The normalized mutual information (NMI) of the contingency matrix ranges from 1 (for an identical pattern) to 0 (for a random correspondence of labels). The NMI, weighted by the basin size, was used as a similarity metric. The similarity between all subject pairs was computed, and compiled in a similarity matrix.

Domain decomposition: The $N \times N$ similarity matrix was projected into a lower-dimensional space using principal component analysis, with M components selected such that the retained variance was above 80%, typically, $M \in \{3,\cdots,10\}$. The resulting data set contained M observations (i.e., the projected components) in N subjects.

Clustering: Multivariate Gaussian mixture models were adapted to projected data (Scrucca et al., 2017). The optimal number of classes C was selected from the maximal Bayesian information criterion. For each

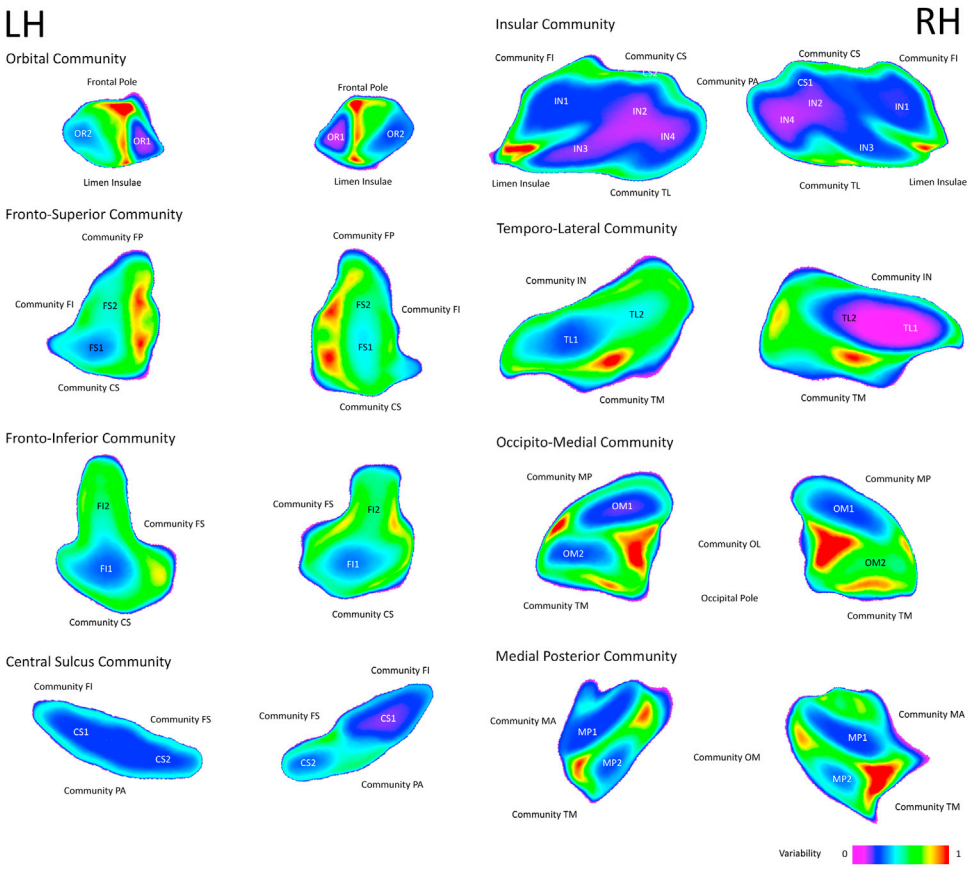

Fig. 4. Variability in example communities OR, FS, FI, CS, IN, TL, OM, and MP. Please refer to Table 2 for anatomical loci of CLVs.

subject, the basin pattern in a specific community was addressed to a community sub-type $c \in \{1, \cdots, C\}$.

Statistical Assessment: In order to assess properties of community sub-types, we computed class-wise maps of the following vertex-wise features: the variability of basin label patterns; cortical depth; cortical curvature; cortical thickness; myelin ratio; and spatial z-score maps of class-wise differences between features. Differences in spatial statistics were considered significant if they passed a Bonferroni correction ($|z| > 4.08$). The complexity of the basin structure was evaluated using linear regression, with the number of basins as the dependent variable, and the sub-type and subject sex as independent variables. Subject age was generally found to have an insignificant influence, so is not reported here.

2.5. Anatomical analysis

Locations of CLVs were determined by searching the overall variability map (Fig. 2, p. 5) for local minima. Vertex positions were mapped back from common into individual space of a reference data set, and anatomical locations identified by comparison with an anatomical atlas (Duvernoy, 1991). For the comparison with fetal development, we referred to the rich collection of photographs of fetal brains in Nishikuni's thesis (2006), where sulcal roots were identified in both hemispheres at different stages of development. The mean time point by which a sulcal root appeared was used in the analysis here. Note that Nishikuni does not report hemispheric asymmetries in development.

3. Results

On the basis of the analytical framework detailed below, we examined the relevance of cortical communities in terms of their relationship to brain development, and their importance for segregating the developing cortex into structural sub-units. First, we studied the relationship between communities and their centers of low variability (CLV). Second, we assessed the relationship of geodesic depth and variability of these centers, and linked their variability to their temporal sequence in fetal brain development. Third, we demonstrated that communities form sub-types, governed by specific properties of CLVs in sub-groups of our cohort.

3.1. Structural centers in communities

A visual comparison of the variability map (Fig. 2, p. 5) with the community map (Fig. 3, p. 6) led to the observation that communities contain core sulcal regions of low variability (in magenta), bordered by variable gyral regions (in red). To study this relationship more systematically, maps of the basin variability in the 13 communities were computed, and their local minima determined as CLVs. Spherical maps were projected to a local plane for visualization (Fig. 4, p. 12). To ease comparison across figures, the same color mapping was used to depict vertex-wise variability measures, although the distinction of some centers may be less apparent.

Community size and number of centers per community were compiled in Table 1. Thirty CLVs were determined in each hemisphere; each community had between one and four centers. Each CLV represents on average 3.1% of the hemispheric surface (2700 mm^2). Notably, centers with a relatively lower variability determine a larger local neighborhood. Their anatomical locations were identified by mapping positions back onto a hemispheric mesh. A list of all centers, their anatomical location, and average variability is compiled in Table 2.

We emphasize that CLVs do not map one-to-one on a sulcal pit. Centers were derived as local minima from a variability map, unlike the process of finding pits as locally deepest surface points (Im et al., 2010; Lohmann et al., 2008). Some centers represent more than one pit,

Table 1
Summary of basic community metrics. Communities: Size (number of vertices (#) and percent of total size (%) in both left and right hemispheres. Low-variability centers (CLVs): Number (#) and percent of total surface size (%). NL refers to non-cortical regions (cut plane areas in the middle and brain stem).

Community	Vertices left		Vertices right		CLVs	
	#	%	#	%	#	%
NL	10531	6.42	10913	6.66	NA	NA
OR	4820	2.94	4658	2.84	2	1.44
FS	9385	5.72	10190	6.21	2	2.98
FI	11223	6.84	11133	6.79	2	3.40
FP	6413	3.91	5111	3.11	1	3.51
CS	7234	4.41	6364	3.88	2	2.07
PA	10733	6.55	16036	9.78	3	2.72
IN	20617	12.58	18113	11.05	4	2.95
TL	17650	10.77	17092	10.43	2	5.21
TM	19648	11.99	21799	13.30	4	3.16
OL	11173	6.81	8916	5.44	2	3.06
OM	13308	8.12	11612	7.08	2	3.80
MA	12210	7.45	9288	5.66	2	3.27
MP	8897	5.43	12617	7.70	2	3.28

Table 2
Locations of CLVs and their relative variability.

Comm.	CLV	Location	Var. left	Var. right
OR	OR1	Olfactory sulcus	low	low
	OR2	Orbital sulcus	medium	medium
FP	FP1	Fronto-marginal sulcus	medium	medium
FS	FS1	Sup. front. sulcus, post.	medium	high
	FS2	Sup. front. sulcus, ant.	high	high
FI	FI1	Inf. front. sulcus, post.	low	low
	FI2	Inf. front. sulcus, ant.	high	high
CS	CS1	Central sulcus, inf.	low	medium
	CS2	Central sulcus, sup.	low	medium
PA	PA1	Post-central sulcus, inf.	medium	medium
	PA2	Post-central sulcus, sup.	high	high
	PA3	Intra-parietal sulcus	medium	medium
IN	IN1	Circular sulcus, front.	medium	medium
	IN2	Circular sulcus, par.	low	low
	IN3	Lat. sulcus, polar plane	low	low
	IN4	Lat. sulcus, temporal plane	low	low
TL	TL1	Sup. temp. sulcus, ant.	medium	low
	TL2	Sup. temp. sulcus, post.	medium	low
TM	TM1	Hippocampal sulcus	low	low
	TM2	Collateral sulcus, mid.	medium	medium
	TM3	Occ.-temp. sulcus, ant.	high	high
	TM4	Inf. temp. sulcus	high	high
OL	OL1	Par.-occ. sulcus	low	low
	OL2	Lat. occ. sulcus	high	high
OM	OM1	Occ.-par. sulcus	low	low
	OM2	Calcarine sulcus	medium	high
MA	MA1	Cingulate sulcus, post.	high	high
	MA2	Cingulate sulcus, ant.	medium	medium
MP	MP1	Cingulate sulcus, asc.	low	low
	MP2	Sub-par. sulcus	medium	medium

because low-variable neighboring basins may coalesce (e.g., TL1, Tl2, FI1, FS2). Combinations of two neighboring sulcal pits lead to different CLV shape configurations (e.g., "I" and "L"-type centers FI1 and FS1).

3.2. Variability vs. geodesic depth

We hypothesized that: (1) There is a close relationship between center variability and depth; (2) Deep, low variable centers are formed early in development. We determined variability and geodesic depth of the 30 CLVs in all individual maps, resulting in a table of N = 1113 subjects by M = 30 variability and depth measures for each hemisphere. Depth measures were normalized by the subject-wise median. Finally, variability and normalized depth were averaged across all subjects.

The variability of CLVs on the right vs. left side is plotted in Fig. 5, top. As the slope of the regression line (1.0005, p < 2e-16) indicates, the

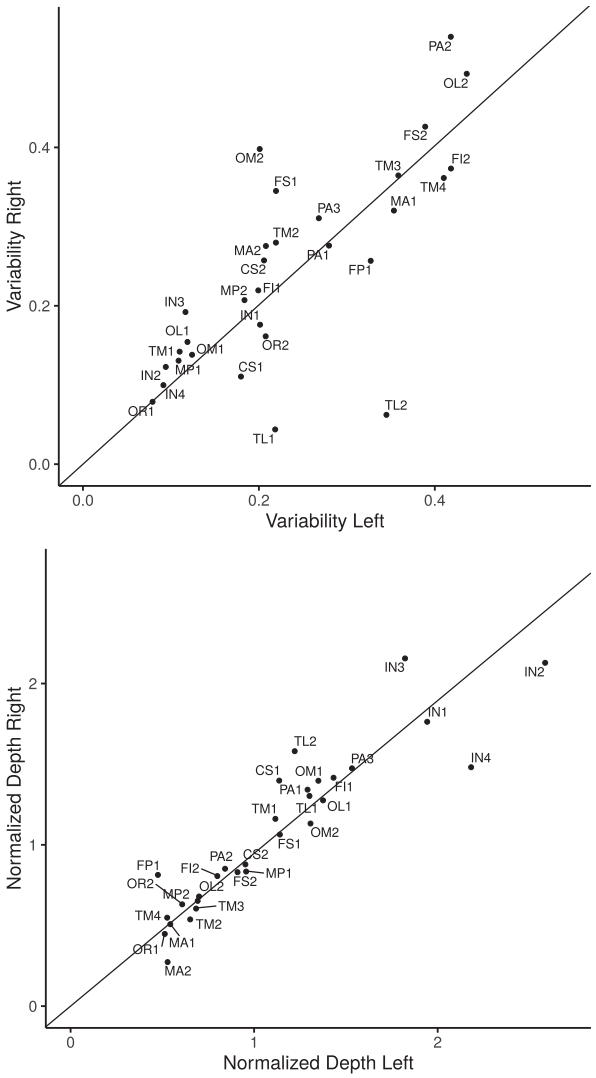

Fig. 5. Top: Variability of CLVs in the right vs. left hemisphere. CLVs OM2, FS1, PA2, and OL2 were less variable on the left, while TL1, TL2, and CS1 were less variable on the right side. Below: Normalized depth of CLVs in the right vs. left hemisphere. Centers were slightly deeper on the left side, with the exception of IN3, TL2, CS1, and FP1. Refer to Table 2 for an explanation of CLV labels.

overall variability was not different between both hemispheres. However, individual variability scores were significantly lower on the left side (Wilcoxon test, p = 0.04). Some CLVs (TL1, TL2, PA2, OM2) showed gross differences in their variability between both hemispheres. Fig. 5, below shows CLV depth on the right vs. left side. Here, the slope of the regression line (0.947, p < 2e-16) indicated that CLVs are overall slightly deeper on the left side. Exceptions are CLVs IN3, TL2, CS1, and FP that are deeper on the right side. Notably, there was a similar group of deep, low-variable centers on both sides (OR1, MP1, TM1, OM1, OL1, IN2-4, plus OR2, IN1, TL1, and TL2 on the right side) that may be considered as the "invariant core" centers of the brain. This group is separated in variability and depth from a second (CS1-FP1) and third group (FP1-OL2).

The assessment of CLV variability vs. normalized depth (Fig. 6) did not reveal a simple relationship. Notably, there was an upper limit on this relationship, because no CLV was deep *and* variable. Separating centers on the basal and medial aspects of the brain (in black) from those on the convexity (in red) demonstrated that variability and depth were strongly correlated for the CLVs on the convexity (left: p = 1.5e-4, $R^2 = 0.56$; right: p = 1.4e-3, $R^2 = 0.44$). Centers on the basal and anterior medial aspect of the brain cannot be deep, due to anatomical constraints.

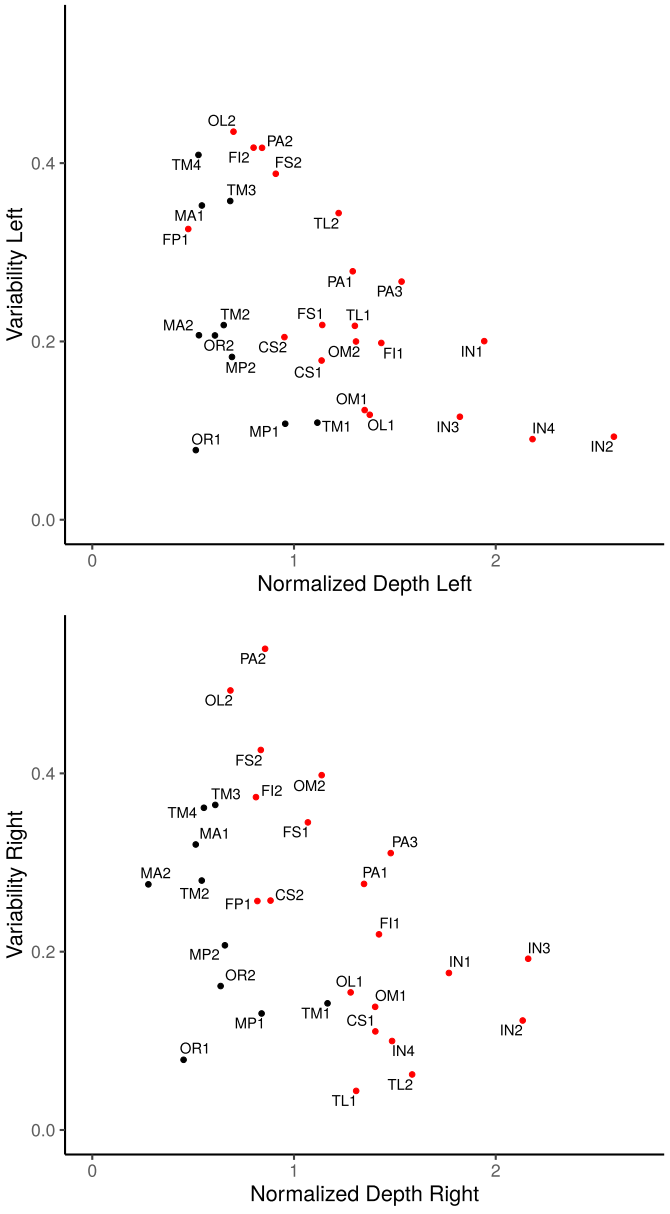

Fig. 6. Variability vs. normalized depth of CLVs in the left and right hemisphere. Centers on the convexity of the brain (in red) showed a strong correlation between variability and depth (left: p = 1.5e-4, $R^2 = 0.56$; right: p = 1.4e-3, $R^2 = 0.44$).

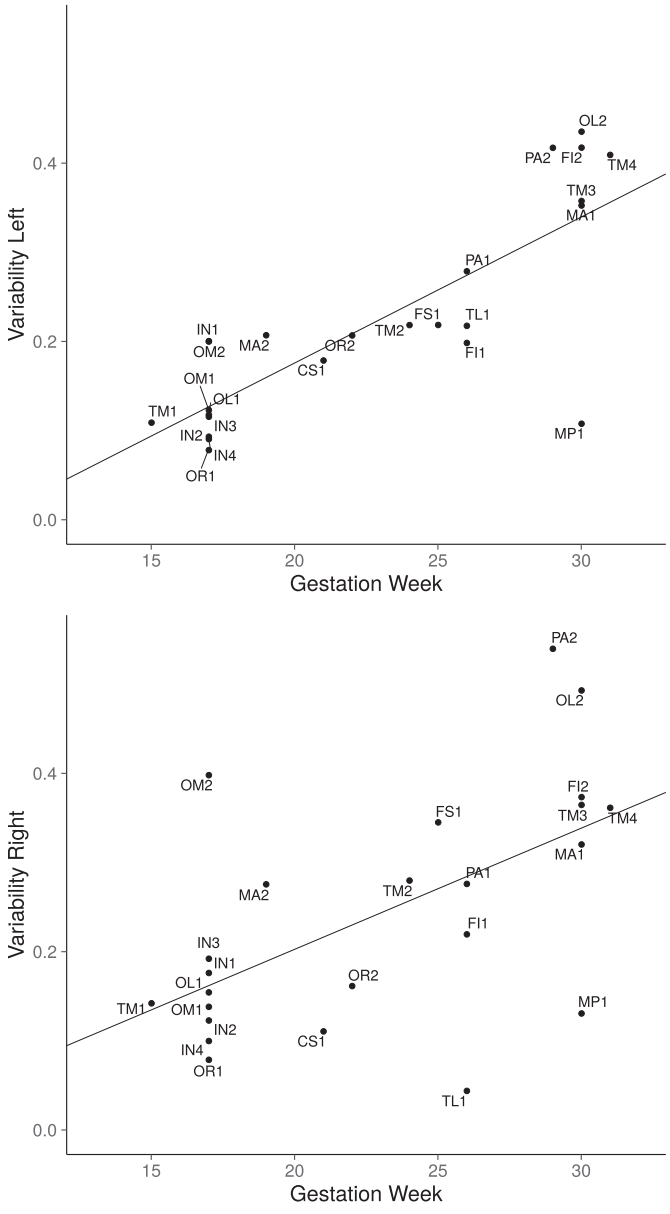

Fig. 7. Variability vs. average timing of sulcal formation (in gestation week) in the left and right hemisphere. Developmental data were adapted from Nishikuni and Ribas (2012). Their data were not separated by hemispheres.

The temporal sequence of emerging folding patterns of the human brain was studied by post-mortem assessment (Chi et al., 1977; Nishikuni, 2006) and in utero MRI (Dubois et al., 2008; Habas et al., 2012; Huang et al., 2013). As previously noted, data about the average appearance of sulci during weeks 12–40 of gestation were taken from (Nishikuni and Ribas, 2012) and adapted to the CLV notation in Table 2. Variability was more strongly correlated with appearance on the left (Fig. 7; left: $R^2 = 0.629$, p = 2.31e-6) than the right side (Fig. 7; right: $R^2 = 0.303$, p = 3.12e-3). Note that post-mortem data (Nishikuni, 2006) were not differentiated by side.

We conclude that sulci appearing early in development remain as regions of low variability in adulthood. The apparent clustering of CLVs into three depth and variability groups spurred the idea that CLVs develop in three "waves": (1) The first wave occurs between GW 16 and 20 and segregates a basal ring of communities (OR, IN, TM, OL, OM, and MA) by seeding one CLV in each community. (2) The second wave follows between GW 21 and 26 as a superior ring of communities (CS, PA, TL, FI, FS, MP, and FP), again, by placing one CLV in each community. At GW 26, CLVs are allocated in all communities. (3) Secondary and ternary structures develop after GW 26. The second CLV appears in each community at the same time (IN, OM) or 4–11 weeks later (OR, OL, TM, MP, MA, FI, PA).

3.3. Community sub-types

The number and pattern of basins within a community differed across subjects. While primary sulci and their roots were regularly found in all subjects, secondary sulci were present only in sub-groups of subjects. Thus, these sub-groups may have distinctive basin patterns within a community, i.e., form structural sub-types. We used the analytic procedure described in Section "Methods" and focused on communities CS, OR, and IN. In comparison with traditional neuroanatomy, these example communities correspond to different hierarchy levels: CS is a sulcus, OR a local region with several sulci, and IN is often considered as a "fifth lobe". Even with the examples at three different scales, we demonstrate that

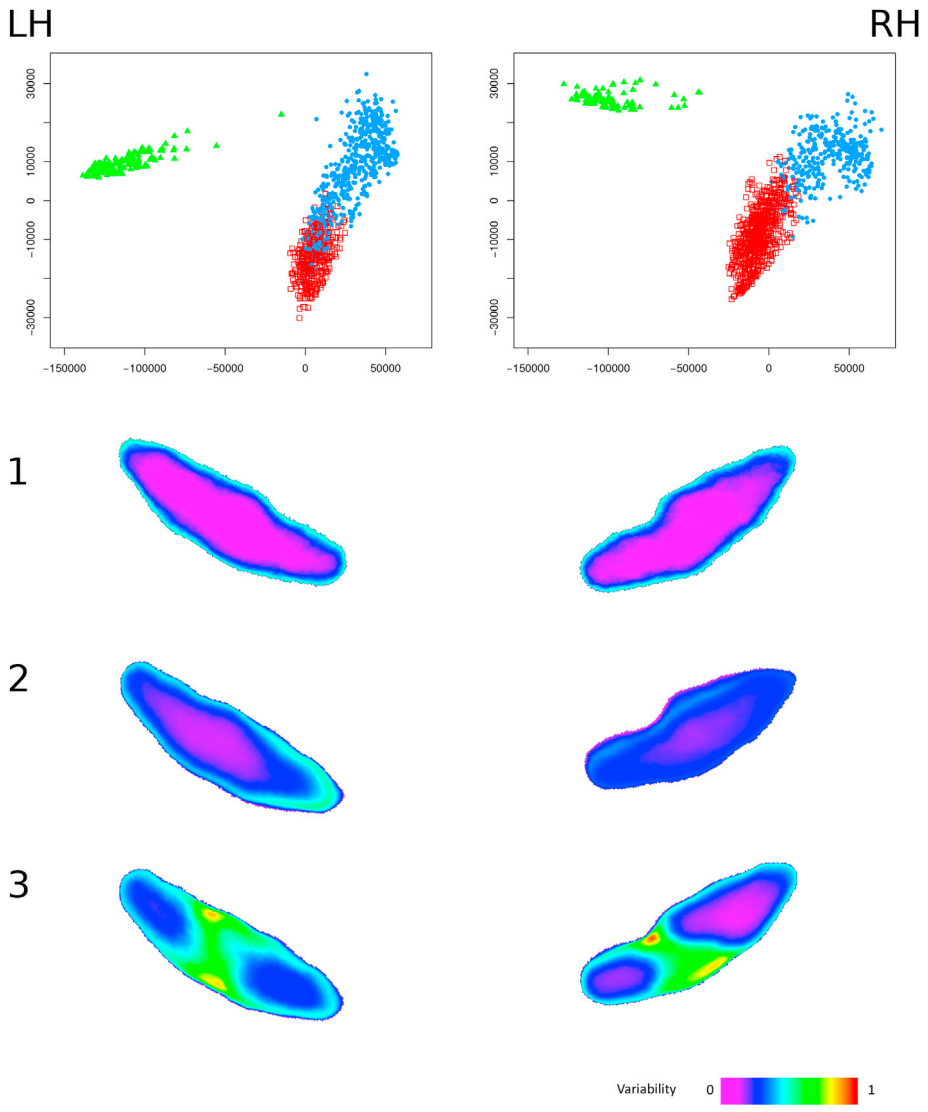

Fig. 8. Sub-types of community CS. Top row: Classification in the left and right hemispheres. Cases marked by green triangles correspond to class 1, blue dots to class 2, and red squares to class 3, shown in the three rows below. Below: Mean variability for the three CS sub-types. In each sub-figure, the outer side corresponds to the inferior, the inner to the superior portion of the central sulcus.

their structural patterning is governed by similar rules.

Community CS - Central Sulcus: We found three sub-types in the CS community that showed highly significant differences in local variability (Fig. 8). In the left hemisphere, type 1 (n = 162 subjects, 14.6%) represented the central sulcus as a single, "straight", deep basin with very low variability (< 0.1). Type 2 (n = 376, 33.8%) split off a more variable portion by a bridging gyrus in its superior third, with a total average of 2.95 basins. In type 3 (n = 575, 51.7%), a bridging gyrus located in the middle separated variable inferior and superior portions. This pattern had 4.07 basins on average. Interestingly, males had 0.29 more basins than females, and the ratio of females in sub-type 1 was significantly higher (1.42, p = 0.042). Similar to the left hemisphere, in the right, type 1 (n = 85, 7.6%) represented the central sulcus as a single, "straight", deep basin with very low variability (< 0.1). Type 2 (n = 343, 30.8%) split off a more variable portion by a bridging gyrus in its superior third, with a total average of 3.24 basins. In type 3 (n = 685, 61.5%), a bridging gyrus was located rather in the middle and separated a variable superior portion. This pattern had 3.56 basins on average. Males had 0.35 more basins than females. A weak association was found between left and right hemispheric clustering (p = 0.059). Types 1–3 were of similar native surface size (left: 3480 mm^2, right: 3251 mm^2). and males had larger areas than females (left: +404 mm^2, p < 2e-16; right: +458 mm^2, p < 2e-16).

Community OR - Orbito-Frontal Cortex: Four sub-types were found in both hemispheres with highly significant differences in local variability (Fig. 9, p. 20). As noted, community OR consists of two CLVs, in the olfactory and orbital sulci. Patterns of sub-types were similar in both hemispheres, and a strong association was found between the left and right hemispheric clustering (p = 1.1e-7).

In type 1 (left: n = 164, 14.7%, 6.31 basins; right: n = 331, 29.7%, 5.98 basins), community OR was comprised of two deep CLVs with very low variability (< 0.1). This type was more prevalent in females (left: 1.40, right: 1.33) and showed a deep transverse orbital sulcus (TOS), with the medial, intermediate, and lateral sulcus typically split off. In type 2 (left: n = 406, 36.5%, 8.40 basins; right: n = 285, 25.6%, 7.51 basins), the CLV in the olfactory sulcus was prominent, while the orbital sulcus was represented by two basins, of which the lateral one was deeper and more invariant. Both sulci were shallower than in sub-type 1. This type was more prevalent in males (left: 1.30, right: 1.64). Type 3 (left: n = 310, 27.9%, 7.39 basins; right: n = 281, 25.2%, 6.90 basins) was similar to type 2, but the CLV in the orbital sulcus was uniformly shallow. In type 4 (left: n = 233, 20.9%, 7.39 basins; right: n = 216, 19.4%, 6.57

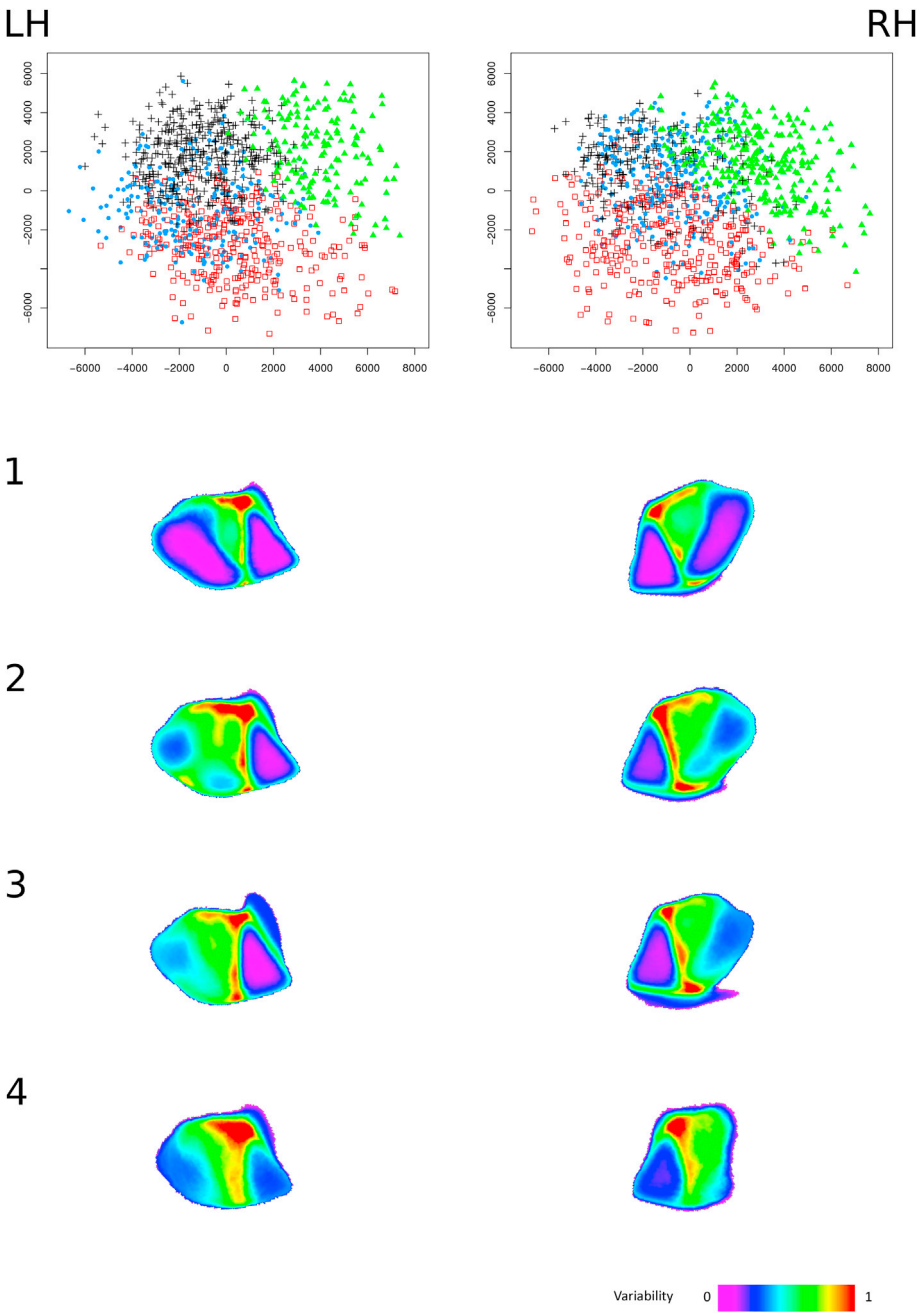

Fig. 9. Sub-types of community OR. Top row: Classification in the left and right hemispheres. Cases marked by green triangles correspond to class 1, blue dots to class 2, red squares to class 3, and black crosses to class 4, shown in the four rows below. Below: Mean variability for the four OR sub-types.

basins), both CLVs were variable and shallow, resulting in a variable basin pattern. Males had significantly more basins than females (left: 0.50, right: 0.59).

In the left hemisphere, types 1 and 4 were of similar native surface size (2827 mm^2 and 2773 mm^2), while types 2 and 3 were significantly larger (3003 mm^2 and 3040 mm^2, p = 1e-9). In the right hemisphere, types 1 and 3 were of similar size (2720 mm^2, 2560 mm^2), while type 2 was significantly larger (2780 mm^2, p = 1e-9) and type 4 smaller (2300 mm^2, p = 1e-9). Independent of sub-type, males had larger areas than females (left: +352 mm^2, p < 2e-16; right: +348 mm^2, p < 2e-16).

Chiavaras and Petrides (2000) developed a classification scheme for orbito-frontal sulci using structural properties as detected by MR imaging. Although their definition was phenomenological, our type 1 corresponded to their type 3, our type 2 to their type 2, and our types 3 and 4 to their type 1.

Community IN - Insula: Four sub-types were found in community IN that showed highly significant differences in local variability (Fig. 10, p. 22). The community IN consisted of four CLVs: in the frontal (IN1) and parietal (IN2) section of the circular sulcus (at the anterior-posterior level of the long insular gyri), and the temporal (IN3) and polar (IN4) planes (at the level of the short insular gyri, with IN3 segregated from IN4 by the transverse temporal gyrus). Note that this definition of the community IN differs from the standard delineation as it includes opercular regions, especially, on the temporal side. The clear distinction between IN1 and IN2 corresponds to the sub-division into anterior insula/frontal operculum and posterior insula/parietal operculum, in line with a recent data-driven analysis of functional neuroimaging data (Kelly et al., 2012).

Sub-type patterns were similar in both hemispheres, and a significant association was found between the left and right hemispheric clustering (p = 3.6e-7). Type 1 (left: n = 357, 32.1%, 8.45 basins; right: n = 315,

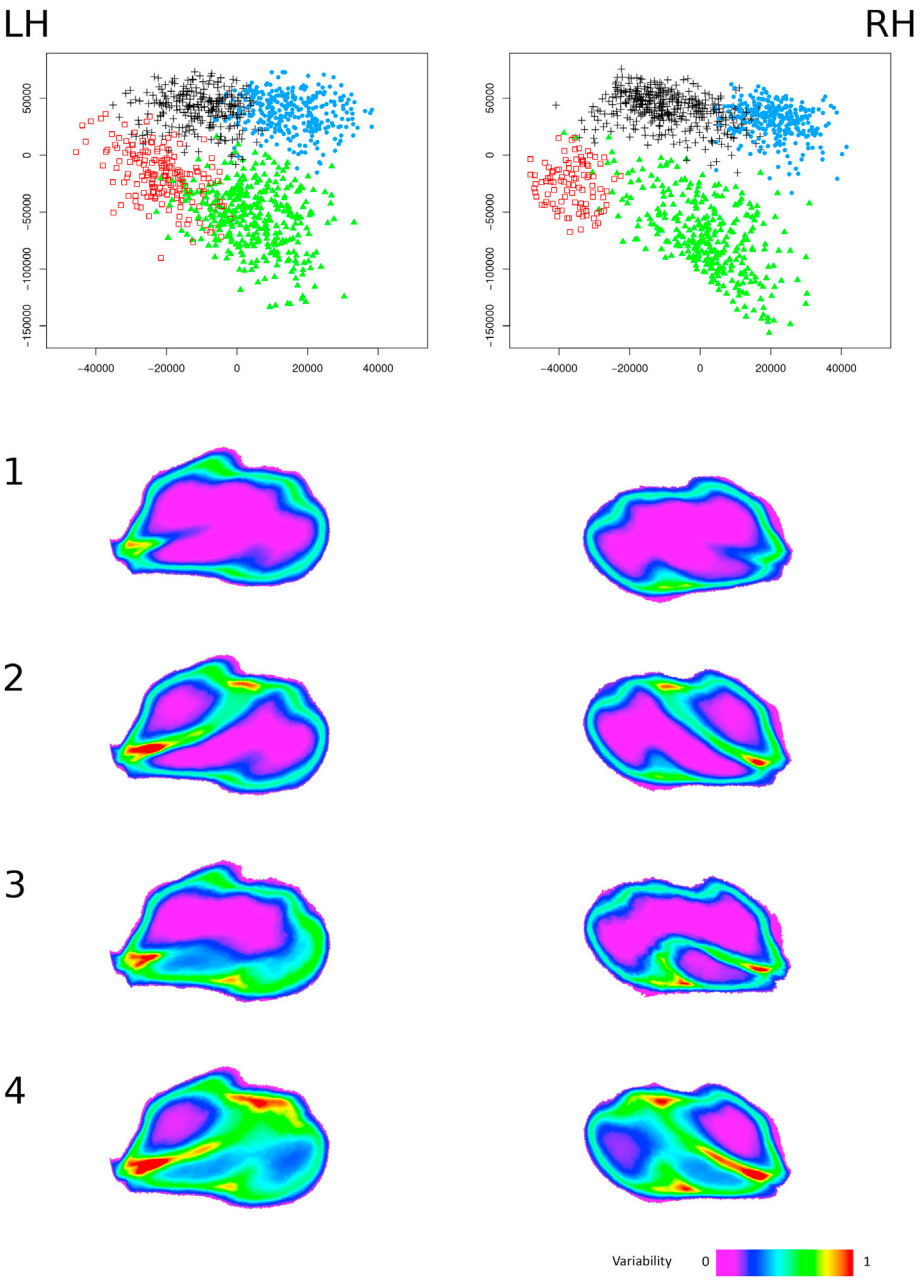

Fig. 10. Sub-types of community IN. Top row: Classification in the left and right hemispheres. Cases marked by green triangles correspond to class 1, blue dots to class 2, red squares to class 3, and black crosses to class 4, shown in the four rows below. Below: Mean variability for the four IN sub-types.

28.3%, 6.86 basins) was found as a single, confluent group of four centers with very low variability (< 0.1). In type 2 (left: n = 257, 23.1%, 10.35 basins; right: n = 387, 34.8%, 7.94 basins), the center in anterior insula/frontal operculum was significantly less deep and more variable, and split off by 1–2 additional basins. Type 3 (left: n = 324, 29.1%, 10.66 basins; right: n = 100, 9.0%, 8.01 basins) showed prominent CLVs in the insula, while the center in the polar plane was more variable, separated by 1–2 additional basins. In type 4 (left: n = 175, 15.7%, 12.33 basins; right: n = 311, 27.9%, 10.19 basins), the anterior insula and polar plane had a low variability, while the other two sub-regions were more shallow, variable and separated by 3–4 additional basins. Males had significantly more basins than females (left: 1.04, right: 0.98, p = 1.7e-3).

In the left hemisphere, types 1, 2 and 3 had similar native surface size (8951 mm^2, 8948 mm^2, and 9104 mm^2), while type 4 was significantly larger (9193 mm^2, p = 0.00195). In the right hemisphere, types 1 and 2 were of similar size (7950 mm^2, 8024 mm^2), while types 3 and 4 were significantly larger (8213 mm^2, p = 0.00221 and 8148 mm^2, p = 0.0072). Independent of sub-type, males had larger areas than females (left: +1131 mm^2, p < 2e-16; right: +876 mm^2, p < 2e-16).

Centers vs. Sub-Type Structure: Based on the structural variation of the sub-types found above, it appears that their CLVs were expressed in two variants (low variable/deep vs. variable/shallow). A combination of their variants governs the sub-type structure: a community with two CLVs can form four sub-types. Denoting a probability p_i that CLV i is in a low-variable state (likewise, $1 - p_i$ for the variable state), sub-type 1 should be found with a probability $p_1\ p_2$ (likewise, sub-type 4 with a probability of $(1 - p_1)\ (1 - p_2)$). Assuming independence of variant probabilities p_1, p_2, their values were determined from the relative sub-type fractions, and were compiled in Table 3. While the assumption of two discrete variants is likely an over-simplification, the similarity of the observed vs. the estimated fractions is striking. Thirty centers per hemisphere span a state space of more than 1 billion (2^{30}) combinations - offering a simple

Table 3
Examination of sub-type fractions in communities OR, IN, and CS in the left and right hemispheres. For each sub-type *ST*, the observed fractions (column *obs.*), the estimated fractions (column *est.*), governed by the two state probabilities p_1, p_2 (column *Parm.*) are shown.

Community	ST	Probability left			Probability right		
		obs.	est.	Parm.	obs.	est.	Parm.
OR	1	0.147	0.154		0.297	0.297	
	2	0.279	0.279	0.356	0.194	0.242	0.551
	3	0.209	0.202	0.433	0.252	0.254	0.538
	4	0.365	0.365		0.256	0.207	
IN	1	0.321	0.321		0.283	0.211	
	2	0.231	0.206	0.609	0.348	0.348	0.377
	3	0.291	0.288	0.527	0.090	0.166	0.559
	4	0.157	0.185		0.279	0.275	
CS	1	0.146	0.148		0.076	0.082	
	2	0.338	0.339	0.304	0.308	0.352	0.188
	3	0.517	0.155	0.487	0.615	0.100	0.433
	–	–	0.356		–	0.420	

explanation for the puzzling structural variability of the cerebral cortex.

4. Discussion

This study aimed at understanding the spatio-temporal determinants of structural segregation and patterning on the human cerebral cortex. We assessed the spatial relationship between regions common to all brains ("communities") and their individual structural variants ("sub-types"), and provided clues about their temporal allocation.

Our principal findings can be summarized as follows: (1) The cortical surface can be subdivided into 13 communities based on macroscopic features. These communities form the common core expressed in all brains. Their allocation on the early cortical surface reserves sufficient space for developing neuro-functional systems. The individual variability is confined within a community. (2) Thirty centers of low variability are found on the cortical surface. Their variability (present in our adult brains) shows a strong positive correlation with the appearance of corresponding sulci during gestation. Centers forming earlier in development induced a higher regularity in a larger local vicinity, while those forming late result in smaller regions of higher variability. A first, basal ring of communities is segregated from GW 16 to 20, followed by a second, superior ring that appears between GW 21 and 26. (3) The layout of basin patterns within a community is governed by 1–4 centers of low variability. Interestingly, communities can be classified into sub-types, depending on the relative variability in each center. It is likely that - at least in part - this variability depends on individual factors influencing the relative timing at which centers within a community are formed during gestation. (4) Sub-types are independent of those in neighboring communities, while there is a weak to strong association with the sub-type of the corresponding community on the contra-lateral side. Sub-types over all communities comprise a pattern library that is capable of explaining a considerable amount of macro-structural variation of the cortex.

Based on the above, it can be of great interest to integrate these findings with the current knowledge about the spatio-temporal development of the human cortex.

4.1. Methodological considerations

The outcome of community sub-typing depends on three components: The selection of features that represent structural properties; the choice of a similarity metric for comparing features between subject pairs; the layout of an analytical strategy for clustering community sub-types based on their mutual similarity. Note that $N \times N$ pair-wise comparisons must be made before clustering, which can be computationally demanding.

We included a rich set of vertex-wise features in this study (basin labels, local curvature, geodesic depth, cortical thickness, and myelin ratio) and used a statistical comparison over the community region as a similarity measure. Our current method did not correct for a possible relative rotation or scaling of individual patterns. Such a correction might improve results shown here, at the expense of a much higher computational cost.

As an alternative to vertex-wise features, basin patterns can be represented as an attributed *geometric* graph (Bandelt and Chepoi, 2008), where nodes correspond to basins and edges to their neighborhood relationships (Yang and Kruggel, 2008). The connectivity and extent of basin nodes bear important information, thus, neighbors can be merged but not flipped. Most commonly, graph edit methods (Billie, 2005; Ferrer and Bunke, 2012) or random walks (Harchaoui and Bach, 2012) can be employed to compute a similarity metric. Spatial features within a community can also be considered as a probability distribution on the sphere, and a Wasserstein ("earth mover's") metric used to rate similarity (Solomon et al., 2015). Due to the much higher computational complexity of these approaches, we performed limited experiments here, and did not a decisive advantage compared to the simple metric above. We continue to work on the implementation of highly efficient and more capable similarity measures.

After all $N \times N$ pair-wise similarities were compiled in a matrix, data were projected into a lower-dimensional and clustered into sub-types. For domain decomposition, we assessed PCA, ICA and kernel PCA (Schölkopf et al., 1998). For classification, we studied using Gaussian mixture models (GMM) (Scrucca et al., 2017), agglomerative and divisive clustering (Kaufman and Rousseeuw, 1990), and evidence accumulation clustering (Fred and Jain, 2005). Due to the overlap between sub-types in clustering space, results varied across methods and their parameters (e.g., the number of retained components). Domain decomposition by PCA followed by GMM classification was chosen as a well-understood and robust approach here. We plan to revise the methodology when more information about the nature of structural differences within communities is available.

Our former work on line representations of sulci and gyri (Lohmann et al., 1997, 1998) was recently re-kindled in the form of a graph representation of gyral crest lines (Chen et al., 2017). While results shown here clearly indicated that gyral features were more variable than sulcal ones, their relative advantage in capturing important individual detail remains to be assessed. More interestingly, a multi-scale representation of cortical curvature (Duan et al., 2018) led to a novel approach for classifying local gyral patterns. Similarly, a recently described method for the spectral decomposition of the cortical folding (Germanaud et al., 2012) led to interesting conclusion about temporal wave dynamics of cortical development (Dubois et al., 2019=). Research on the representation of individual cortical features and their analytic approaches is on-going (Mangin et al., 2010).

4.2. Community sub-types

A clear clustering was found in communities CS, OR, and IN. Similar results (i.e., two to six clusters) were obtained for other communities, corroborating the hypothesis that combinations of basin patterns within a community cluster to form sub-types. A few results from this analysis deserve a closer look: Hemispheric asymmetries: Overall, the cortex in the right hemisphere appeared to be structurally more complex. Cortical variability was slightly but significantly higher on the right side, and sub-type patterns were less discriminative. Generally, a weak to strong statistical association was found between the sub-type and hemispheric side. Thus, structural features between homologue communities are generally similar but not identical. In contrast, no significant association was found between clusters of neighboring (ipsi-lateral) communities, underlining their structural independence. We interpret that this independence is due to an early segregation in development, as further discussed below. Although there are no striking differences in the cortical development of both hemispheres (Chi et al., 1977; Nishikuni, 2006; Nishikuni and Ribas, 2012; Dubois et al., 2019), early minute

asymmetries become more prominent with time (Im et al., 2010; Habas et al., 2012; Dubois et al., 2014; le Guen et al., 2018b). The strongest hemispheric difference was found for the superior temporal sulcus, which was less variable and deeper on the right side, confirming prior findings (Im et al., 2010; Habas et al., 2012). In contrast to developmental studies by Nishikuni (2006), Chi et al. (1977) reported that the superior temporal sulcus appeared 1–2 weeks earlier on the right side. In addition, the asymmetric development of the transverse temporal gyrus (Chi et al., 1977) leads to more left-sided sulcal interruptions (le Guen et al., 2018b), and thus, to a higher variability. The lateral sulcus is longer on the left, providing more space on its posterior end (IN2, IN4) for the planum temporale (Chi et al., 1977; Im et al., 2010). Chi et al. (1977) also reported an earlier appearance of the superior frontal sulcus on the left side, which was found here as less variable on the left.

Sex differences: Several imaging studies established the fact that brain size scales with body height (e.g., Kruggel, 2006) which largely explains sex-related difference in absolute brain size. In this cohort, body height and sex explained 45% of the overall variance: Males had slightly larger brains (+111 ml, $p < 2e\text{-}16$), with a sex-independent increase in brain volume of 3.2 ml per cm body height ($p = 2.7e\text{-}16$). Our approach for spatial normalization partially corrected for such differences. Males had consistently between 0.3 and 1.0 more basins per community than females, given a male brain surface that is 13.5% larger on average. As previously reported (Kruggel, 2018), these additional basins were small-to medium-sized ($< 400\,mm^2$) and occupied additional space available on the slightly larger male hemisphere. These additional basins did not noticeably influence sub-type configurations. This finding is in line with a former analysis of the cortical folding by Awate et al. (2010) who concluded that patterns in both sexes are not simply scaled versions of each other: While females had a larger number of fine-scale features, males had additional folds. Overall sex differences may also be present in the form of a higher sulcal tortuosity in males (Germanaud et al., 2012; Fish et al., 2017) which is difficult to relate to our analysis. Generally, sex differences were not reported or detected before GW 30 (Scott et al., 2011) but were present in neonates (Meng et al., 2014), which may indicate that influences of sex on brain structure increase with later stages of maturation. A highly significant association between sub-type and sex was found for some communities (e.g., CS type 1 left, OR type 1 and 2). Interestingly, a recent voxel-based study of multi-modal MRI brain data (Feis et al., 2013) revealed the most significant sex-related differences in the fronto-orbital and fronto-inferior portions of the brain. Thus, it is likely that sex-related differences become more prevalent when focusing on sub-regions, such as communities, which is under further investigation.

Age-related changes: Our cohort included adults in the age range between 20 and 36. Especially the frontal cortex is known to still mature in early adulthood (Sowell et al., 1999), while degenerative processes become noticeable in the fourth decade of life (Kruggel, 2006). Longitudinal studies in infants (Duan et al., 2018; Dubois et al., 2008; Meng et al., 2014) described macroscopic correlates of cortical maturation as an increase of gyral fine-structure. Changes were quantified by a higher fractal dimension of the cortical folding (Sandu et al., 2014) or an increase of the proportion of higher frequencies in a spatial decomposition of surface curvature (Dubois et al., 2019; Germanaud et al., 2012). Degenerative processes beginning in adulthood lead to a thinning of the cortex and white matter stalks, thereby reducing gyral fine-structure. In contrast, sulcal pits are considered as cortical landmarks that remain stable throughout life (Meng et al., 2014).

Wherever applicable, we controlled measures for a possible dependence of age. Surprisingly, we did not find influences at a significance level stronger than a trend, so they were not reported here. We remark that 70% of subjects in our cohort belong to the age range of 25–32 years, which may be considered as the "plateau phase" in the transition between maturation and degeneration. In the context of our analysis, changes in gyral fine-structure may correspond to changes in detail of boundaries between adjacent basins, but not to changes in their spatial arrangement. Thus, we expect that aging affects local quantitative measures (e.g., variability), but not regional features (e.g., the community subclass type).

4.3. Relation to brain development and genetics

This study determined a strong correlation between the variability of centers and the temporal sequence of their appearance during fetal development. In the past, the development of macroscopic structural features has received much attention: Seminal work was performed the 19th century (Gratiolet, 1854; Eberstaller, 1890; Cunningham, 1892), although reports were rather descriptive and obtained from limited sample sizes. More recent post-mortem examinations were based on larger samples (Chi et al., 1977; Nishikuni, 2006; Nishikuni and Ribas, 2012) and complemented by image-analytic methods applied to in utero MRI (Dubois et al. 2008, 2014; Hu et al., 2011; Clouchoux et al., 2012; Habas et al., 2012). Nishikuni and Ribas (2012) attributed some variability in results vary due to: (1) Difficulties in determining the exact date of contraception; (2) Increasing individual biological variation of sulcus formation during gestation; (3) Method-related detection criteria. However, there is converging evidence for the relative sequence of sulcus formation which was assessed here (Nishikuni and Ribas, 2012). While it was hypothesized before that sulcal pits are presumably formed early (Regis et al., 1995; Lohmann et al., 2008; Im et al., 2010), we presented here, to our best knowledge, the first quantitative evidence for this hypothesis.

Brain development comes in waves. The apparent grouping of CLVs by variability and depth (Fig. 5), and their correlation with development (Fig. 6) support the idea of three "waves". A first, basal ring of communities is segregated during GW 16–20 by seeding a single CLV in each community. A second, superior ring follows between GW 21 and 26. Around this time point, all communities are allocated. A second CLV is placed typically 4–11 weeks after the first one, and is rather related to the development of secondary features. We note that the first ring corresponds to phylogenetically old cortical areas, while the second ring consists of more recent ones.

The knowledge about the microscopic development of the human brain dramatically increased in recent years (for recent reviews, refer to: Sun and Hevner, 2014; Fernandez et al., 2016; Borrell, 2018). Several mechanisms were determined as pre-conditions for the folding of the human cortex: (1) Abundant neurogenesis and gliogenesis (Welker, 1990); (2) Splitting of the subventricular zone (SVZ) into inner and outer sections (OSVZ) during neurogenesis (Reillo et al., 2011); (3) Complex morphological and transcriptional diversity of progenitor cells (de Juan Romero et al., 2015); (4) Regional differences in the density of progenitor cell proliferation (Reillo et al., 2011) and gene expression levels (de Juan Romero et al., 2015). The regularity of macroscopic folding patterns within and across species suggest the existence of genetic mechanisms that regulate early cortical development (Borrell, 2018). A transcriptomics analysis in the developing ferret determined many genes expressed in distinct spatial patterns (Huang et al., 2013; de Juan Romero et al., 2015) and temporal variations (Martinez-Martinez et al., 2016) in the OSVZ that are related to prospective locations of primary folds and fissures. Jammes and Gilles (1983) studied the growth of the surface area in human fetuses. They found a biphasic growth, with a slow gain of the isocortex up to GW 24–26 and an exponential growth thereafter. Conversely, the allocortex showed a regular gain in GW 13–31, with no increase later on. Likewise, the germinal matrix (SVZ and ISVZ) peaked in size at GW 25, then showed a marked decrease. These findings are similar to a later MRI-based study (Scott et al., 2011), who modeled isocortical growth as exponential from GW 20 on. Thus, the assumed formation of our CLVs in two stages (GW 16–20 and 21–26) precedes and prepares for the period of cortical growth, corroborating their importance for spatial segregation.

Details of the genetic regulation underlying the spatio-temporal pattern formation of the human cortex are still largely unknown.

However, recent studies demonstrated the heritability of 16 sulcal pits that correspond to our CLVs (le Guen et al., 2018ale Guen et al., 2018b). Further evidence for the influence of genetic factors may come from the assessment of specific types of brain malformations (Mangin et al., 2010; Im and Grant, 2018).

Several groups investigated the hypothesis that gyrification is a consequence of differential mechanical forces that occur during cortical growth (e.g., Bayly et al., 2013; Ronan et al., 2014; Tallinen et al., 2016; Toro and Burnod, 2005; Xu et al., 2010). Bionumerical simulations of a developing brain consisting of a cortical layer attached to a white matter core led to brain models that stunningly match an adult brain (Tallinen et al., 2016).

It is likely that both genetics and biomechanics contribute to gyrification. While genetic mechanisms described above may indicate locations and time lines of gyrification, they do not suggest *why* gyrification occurs - and biomechanical processes may offer an explanation. Conversly, a pure biomechanical model may be insufficient to explain why the complex-shaped brain is formed in a highly similar fashion - a spatio-temporal control likely stears brain growth.

4.4. Determinants of cortical variability

An early segregation of cortical space is required to ensure a regular development. We assume that the cortical communities detected in adults correspond to these regions. Their allocation is presumably genetically determined and common to all human brains. The cortical folding process is regularized by a temporal sequence of seeding centers within communities, with a first, early set in phylogenetically older regions, and a later set in younger regions. Centers formed early induce a larger, locally more regular folding pattern, while those forming later influence smaller areas with a higher degree of variability. The relative formation of centers within a community leads to distinct structural patterns that are detectable as community sub-types. The spatio-temporal pattern of center development is also presumably genetically determined, but to a lesser extent than the community segregation process and/or controlled by genetic variants common to sub-groups of a populations. Non-genetic factors contribute to the individual cortical formation with increasing weight from the third trimester on.

Options for “assembling cortices” by combining sub-types of the 13 communities may explain some of the puzzling individual cortical variability. The regular portion of the conventional neuro-anatomical ontology maps to the layout of the community structure and their inherent invariants. Individual structural variants are confined within a community, and are often not described in anatomical terms, because a suitable comprehensive framework is missing.

We emphasize that the sub-typing conducted here is based on macroscopic assessment of structural features only. Further evidence must come from the inclusion of structural connectivity and functional results, and will likely lead to even more fine-grained sub-division of cortical regions (e.g., Kringelbach and Rolls, 2004; Anwander et al., 2007; Uylings et al., 2010; Kahnt et al., 2012, Kelly et al., 2012). Thus, we prefer to refrain from speculating about neuro-biological implications of regional sub-typing at this time. Considering the strong arguments for region sub-types provided by this data-driven analysis, we suggest to consider advantages of individual sub-typing into account when analyzing structure-function relationships in the human brain.

Acknowledgment

Authors thank Dr. Robert Hunt (Depts. of Anatomy and Neurobiology, UC Irvine) for insightful comments on the manuscript.

Appendix A. Supplementary data

Supplementary data to this article can be found online at https://doi.org/10.1016/j.neuroimage.2019.04.031.

References

Anwander, A., Tittgemeyer, M., von Cramon, D.Y., Friederici, A.D., Knösche, T.R., 2007. Connectivity-based parcellation of Broca's area. Cerebr. Cortex 17, 816–825.
Awate, S.P., Yushkevich, P.A., Song, Z., Licht, D.J., Gee, J.C., 2010. Cerebral cortical folding analysis with multivariate modeling and testing: studies on gender differences and neonatal development. Neuroimage 53, 450–459.
Bandelt, H.J., Chepoi, V., 2008. Metric graph theory and geometry: a survey. Contemp. Math. 453, 49–86.
Bayly, P.V., Okamoto, R.K., Xu, G., Shi, Y., Taber, L.A., 2013. A cortical folding model incorporating stress-dependent growth explains gyral wavelengths and stress patterns in the developing brain. Phys. Biol. 10, 016005.
Billie, P., 2005. A survey on tree edit distance and related problems. Theor. Comput. Sci. 337, 217–239.
Borrell, V., 2018. How cells fold the cerebral cortex. J. Neurosci. 38, 776–783.
Campigotto, R., Conde-Cespedes, P., Guillaume, J.L., 2014. A generalized and adaptive method for community detection arVix:1406.2518v1.
Chen, H., Li, Y., Ge, F., Li, G., Shen, D., Liu, T., 2017. Gyral net: a new representation of cortical folding organization. Med. Image Anal. 42, 14–25.
Chi, J.G., Dooling, E.C., Gilles, F.H., 1977. Gyral development of the human brain. Ann. Neurol. 1, 86–93.
Chiavaras, M.M., Petrides, M., 2000. Orbitofrontal sulci of the human and macaque monkey brain. J. Comp. Neurol. 422, 35–54.
Clouchoux, C., Kudelski, D., Gholipour, A., Warfield, S.K., Viseur, S., Bouyssi-Kobar, M., Mari, J.L., Evans, A.C., du Plessis, A.J., Limperopoulos, C., 2012. Quantitative in vivo MRI measurement of cortical development in the fetus. Brain Struct. Funct. 217, 127–139.
Cunningham, D.J., 1892. Contribution to the Surface Anatomy of the Cerebral Hemispheres. Academy House, Dublin, Ireland.
de Juan Romero, C., Bruder, C., Tomasello, U., Sanz-Anquela, J.M., Borrell, V., 2015. Discrete domains of gene expression in germinal layers distinguish the development of gyrencephaly. EMBO J. 34, 1859–1874.
Desikan, R.S., Segonne, F., Fischl, B., Quinn, B.T., Dickerson, B.C., Blacker, D., Buckner, R.L., Dale, A.M., Maguire, R.P., Hyman, B.T., Albert, M.S., Killiany, R.J., 2006. An automated labeling system for subdividing the human cerebral cortex on MRI scans into gyral based regions of interest. Neuroimage 31, 968–998.
Duan, D., Xia, S., Rekik, I., Meng, Y., Wu, Z., Wang, L., Lin, W., Gilmore, J.H., Shen, D., Li, G., 2018. Exploring folding patterns of infant cerebral cortex based on multi-view curvature features: methods and applications. Neuroimage. https://doi.org/10.1016/j.neuroimage.2018.08.041.
Dubois, J., Benders, M., Borradori-Tolsa, C., Cachia, A., Lazeyras, F., Ha-Vinh Leuchter, R., Sizonenko, S.V., Warfield, S.K., Mangin, J.F., Hüppi, P.S., 2008. Primary cortical folding in the human newborn: an early marker of later functional development. Brain 2028–2041. https://doi.org/10.1093/brain/awn137.
Dubois, J., Dehaene-Lambertz, G., Kulikova, S., Poupon, C., Hertz-Pannier, L., 2014. The early development of the brain white matter: a review of imaging studies in fetuses, newborns and infants. Neuroscience 276, 48–71.
Dubois, J., Lefevre, J., Angleys, H., Leroy, F., Fischer, C., Lebenberg, J., Dehaene-Lambertz, G., Borradori-Tolsa, C., Lazeyras, F., Hertz-Pannier, L., Mangin, J.F., Hüppi, P.S., Germanaud, D., 2019. The dynamics of cortical folding waves and prematurity-related deviations revealed by spatial and spectral analysis of gyrification. Neuroimage. https://doi.org/10.1016/j.neuroimage.2018.03.005.
Duvernoy, H.M., 1991. The Human Brain. Springer, Wien, Austria.
Eberstaller, O., 1890. Das Stirnhirn: Ein Beitrag zur Anatomie der Oberfläche des Grosshirns. Urban & Schwarzenberg, Leipzig, Germany.
Feis, D.L., Brodersen, K.H., von Cramon, D.Y., Luders, E., Tittgemeyer, M., 2013. Decoding gender dimorphism of the human brain using multimodal anatomical and diffusion MRI data. Neuroimage 70, 250–257.
Fernandez, V., Llinares-Benadero, C., Borrell, V., 2016. Cerebral cortex expansion and folding: what have we learned? EMBO J. https://doi.org/10.15252/embj.201593701.
Ferrer, M., Bunke, H., 2012. Graph edit distance - theory, algorithms, and applications. In: Lezoray, O., Grady, L. (Eds.), Image Processing and Analysis with Graphs: Theory and Practice. CRC Press, Boca Raton, USA, pp. 383–422.
Fish, A.M., Cachia, A., Fischer, C., Mankiw, C., Reardon, P.K., Clasen, L.S., Blumenthal, J.D., Greenstein, D., Giedd, J.N., Mangin, J.F., Raznahan, A., 2017. Influences of brain size, sex, and sex chromosome complement on the architecture of human cortical folding. Cerebr. Cortex 27, 5557–5567.
Fortunato, S., 2008. Community detection in graphs. Phys. Rep. 486, 75–174.
Fred, A.L.N., Jain, A.K., 2005. Combining multiple clusterings using evidence accumulation. IEEE Trans. Pattern Anal. Mach. Intell. 27, 835–850.
Germanaud, D., Lefevre, J., Toro, R., Fischer, C., Dubois, J., Hertz-Pannier, L., Mangin, J.F., 2012. Larger is twistier: spectral analysis of gyrification (SPANGY) applied to adult brain size polymorphism. Neuroimage 63, 1257–1272.
Germann, J., Robbins, S., Halsband, U., Petrides, M., 2005. Precentral sulcal complex of the human brain: morphology and statistical probability maps. J. Comp. Neurol. 493, 334–356.
Glasser, M.F., van Essen, D.C., 2011. Mapping human cortical areas in vivo based on myelin content as revealed by T1- and T2-weighted MRI. J. Neurosci. 31, 11597–11616.
Glasser, M.F., Coalson, T.S., Robinson, E.C., Hacker, C.D., Harwell, J., Yacoub, E., Ugurbil, K., Andersson, J., Beckmann, C.F., Jenkinson, M., Smith, S.M., van Essen, D.C., 2016. A multi-modal parcellation of human cerebral cortex. Nature 536, 171–178.
Gratiolet, L.P., 1854. Memoire sur les plis cerebraux de l’homme et des primates. Bertrand, Paris, France.

Habas, P.A., Scott, J.A., Roosta, A., Rajagopalan, V., Kim, K., Rousseau, F., Barkovich, A.J., Glenn, O.A., Studholme, C., 2012. Early folding patterns and asymmetries of the normal human brain detected from in utero MRI. Cerebr. Cortex 22, 13–25.

Harchaoui, Z., Bach, F., 2012. Tree-walk kernels for computer vision. In: Lezoray, O., Grady, L. (Eds.), Image Processing and Analysis with Graphs: Theory and Practice. CRC Press, Boca Raton, USA, pp. 499–528.

Hu, H.H., Hung, C., Wu, Y.T., Chen, H.Y., Hsieh, J.C., Guo, W.Y., 2011. Regional quantification of developing human cortical shape with a three-dimensional surface-based magnetic resonance imaging analysis in utero. Eur. J. Neurosci. 34, 1310–1319.

Huang, H., Jeon, T., Sedmak, G., Pletikos, M., Vasung, L., Xu, X., Yarowsky, P., Richards, L.J., Kostovic, I., Sestan, N., Mori, S., 2013. Coupling diffusion imaging with histological and gene expression analysis to examine the dynamics of cortical areas across the fetal period of human brain development. Cerebr. Cortex 23, 2620–2631.

Human Connectome Project, 2017. 1200 Subjects Data Release Reference Manual. https://www.humanconnectome.org/study/hcp-young-adult/document/1200-subjects-data-release. (Accessed 14 November 2018).

Im, K., Grant, P.E., 2018. Sulcal pits and patterns in developing human brains. Neuroimage. https://doi.org/10.1016/j.neuroimage.2018.03.057.

Im, K., Jo, H.J., Mangin, J.F., Evans, A.C., Kim, S.I., Lee, J.M., 2010. Spatial distribution of deep sulcal landmarks and hemispherical asymmetry on the cortical surface. Cerebr. Cortex 20, 602–611.

Jammes, J., Gilles, F., 1983. Telencephalic development: matrix volume and isocortex and allocortex surface areas. In: Gilles, F., Leviton, A., Dooling, E. (Eds.), The Developing Human Brain: Growth and Epidemiologic Neuropathology. Elsevier, Amsterdam, The Netherlands, pp. 87–93.

Kahnt, T., Chang, L.J., Park, S.Q., Heinzle, J., Haynes, J.D., 2012. Connectivity-based parcellation of the human orbitofrontal cortex. J. Neurosci. 32, 6240–6250.

Kaufman, L., Rousseeuw, P.J., 1990. Finding Groups in Data: an Introduction to Cluster Analysis. Wiley, New York, USA.

Kelly, C., Toro, R., Martino, A.C., Cox, C.L., Bellec, P., Castellanos, F.X., Milham, M.P., 2012. A convergent functional architecture of the insula emerges across imaging modalities. Neuroimage 61, 1129–1142.

Kringelbach, M.L., Rolls, E.T., 2004. The functional neuroanatomy of the human orbitofrontal cortex: evidence from neuroimaging and neuropsychology. Prog. Neurobiol. 72, 341–372.

Kruggel, F., 2006. MRI-based volumetry of head compartments: normative values of healthy adults. Neuroimage 30, 1–11.

Kruggel, F., 2008. Robust parametrization of brain surface meshes. Med. Image Anal. 12, 291–299.

Kruggel, F., 2018. The macro-structural variability of the human neocortex. Neuroimage 172, 620–630.

le Guen, Y., Auzias, G., Leroy, F., Noulhiane, M., Dehaene-Lambertz, G., Duchesnay, E., Mangin, J.F., Coulon, O., Frouin, V., 2018a. Genetic influence on the sulcal pits: on the origin of the first cortical folds. Cerebr. Cortex 28, 1922–1933.

le Guen, Y., Leroy, F., Auzias, G., Riviere, D., Grigis, A., Mangin, J.F., Coulon, O., Dehaene-Lambertz, G., Frouin, V., 2018b. The chaotic morphology of the left superior temporal sulcus is genetically constrained. Neuroimage 174, 297–307.

Lohmann, G., 1998. Extracting line representations of sulcal and gyral patterns in MR images of the human brain. IEEE Trans. Med. Imaging 17, 1040–1048.

Lohmann, G., Kruggel, F., von Cramon, D.Y., 1997. Automatical detection of sulcal bottom lines in MR images of the human brain. In: Duncan, J., Gindi, G. (Eds.), Information Processing in Medical Imaging (Poultney), Lecture Notes in Computer Science, vol. 1230. Springer, Heidelberg, pp. 369–374.

Lohmann, G., von Cramon, D.Y., Colchester, A.C., 2008. Deep sulcal landmarks provide an organizing framework for human cortical folding. Cerebr. Cortex 18, 1415–1420.

Mangin, J.F., Jouvent, E., Cachia, A., 2010. In-vivo measurement of cortical morphology: means and meanings. Curr. Opin. Neurol. 23, 359–367.

Martinez-Martinez, M.A., de Juan Romero, C., Fernandez, V., Cardenas, A., Götz, M., Borrell, V., 2016. A restricted period for formation of outer subventricular zone defined by Cdh1 and Trnp1 levels. Nat. Commun. 7, 11812.

Meng, Y., Li, G., Lin, W., Gilmore, J.H., Shen, D., 2014. Spatial distribution and longitudinal development of deep cortical sulcal landmarks in infants. Neuroimage 100, 206–218.

Nishikuni, K., 2006. Estudo do desenvolvimento morfologico fetal e pos-natal dos sulcos cerebrais [in Portugese]. Thesis, University of Sao Paulo, Brazil.

Nishikuni, K., Ribas, G.C., 2012. Study of fetal and postnatal morphological development of the brain sulci. J. Neurosurg. Pediatr. 11, 1–11.

Oishi, K., Zilles, K., Amunts, K., Faria, A., Jiang, H., Li, X., Akhter, K., Hua, K., Woods, R., Toga, A.W., Pike, G.B., Rosa-Neta, P., Evans, A., Yhang, J., Huang, H., Miller, M.I., van Zijl, P.C.M., Mazziotta, J., Mori, S., 2008. Human brain white matter atlas: identification and assignment of common anatomical structures in superficial white matter. Neuroimage 43, 447–457.

Ono, M., Kubik, S., Abernathey, C.D., 1990. Atlas of the Cerebral Sulci. Thieme, Stuttgart, Germany.

Osechinskiy, S., Kruggel, F., 2012. Cortical surface reconstruction from high-resolution MR brain images. Int. J. Biomed. Imaging. https://doi.org/10.1155/2012/870196.

Regis, J., Mangin, J.F., Frouin, V., Sastre, F., Peragut, J.C., Samson, Y., 1995. Generic model for the localization of the cerebral cortex and preoperative multimodal integration in epilepsy surgery. Stereotact. Funct. Neurosurg. 65, 72–80.

Regis, J., Mangin, J.F., Ochiai, T., Frouin, V., Riviere, D., Cachia, A., Tamura, M., Samson, Y., 2005. "Sulcal root" generic model: a hypothesis to overcome the variability of the human cortex folding patterns. Neurol. Med.-Chir. 45, 1–17.

Reillo, I., de Juan Romero, C., Garcia-Cabezas, M.A., Borrell, V., 2011. A role for intermediate radial glia in the tangential expansion of the mammalian cerebral cortex. Cerebr. Cortex 21, 1674–1694.

Ronan, L., Voets, N., Rua, C., Alexander-Bloch, A., Hough, M., Mackay, C., Crow, T.J., James, A., Giedd, J.N., Fletcher, P.C., 2014. Differential tangential expansion as a mechanism for cortical gyrification. Cerebr. Cortex 24, 2219–2228.

Sandu, A.L., Izard, E., Specht, K., Beneventi, H., Lundervold, A., Ystad, M., 2014. Post-adolescent developmental changes in cortical complexity. Behav. Brain Funct. 2014, 10–44.

Schölkopf, B., Smola, A., Müller, K.R., 1998. Nonlinear component analysis as a kernel eigenvalue problem. Neural Comput. 10, 1299–1319.

Scott, J.A., Habas, P.A., Kim, K., Rajagopalan, V., Hamzelou, K.S., Corbett-Detig, J.M., Barkovich, A.J., Glenn, O.A., Studholme, C., 2011. Growth trajectories of the human fetal brain tissues estimated from 3D reconstructed in utero MRI. Int. J. Dev. Neurosci. 29, 529–536.

Scrucca, L., Fop, M., Murphy, T.B., Raftery, A.E., 2017. Mclust 5: clustering, classification and density estimation using Gaussian finite mixture models. The R Journal 8, 205–233.

Solomon, J., de Goes, F., Peyre, G., Cuturi, M., Butscher, A., Nguyen, A., Du, T., Guibas, L., 2015. Convolutional Wasserstein distances. ACM Trans. Graph. 34, 66, 1–66:11.

Sowell, E.R., Thompson, P.M., Holmes, C.J., Jernigan, T.L., Toga, A.W., 1999. In vivo evidence for post-adolescent brain maturation in frontal and striatal regions. Nature Neurosci. 1999, 859–861.

Sun, T., Hevner, R.F., 2014. Growth and folding of the mammalian cerebral cortex: from molecules to malformations. Nat. Rev. Neurosci. 15, 217–232.

Swanson, L., 2015. Neuroanatomical Terminology: A Lexicon of Classical Origins and Historical Foundations. Oxford University Press, Oxford, United Kingdom.

Tallinen, T., Chung, J.Y., Rousseau, F., Girard, N., Lefevre, J., Mahadevan, L., 2016. On the growth and form of cortical convolutions. Nat. Phys. 12, 588–593.

Tomaiuolo, F., MacDonald, J.D., Caramanos, Z., Posner, G., Chiavaras, M., Evans, A.C., Petrides, M., 1999. Morphology, morphometry and probability mapping of the pars opercularis of the inferior frontal gyrus: an in vivo MRI analysis. Eur. J. Neurosci. 11, 3033–3046.

Toro, R., Burnod, Y., 2005. A morphogenetic model for the development of cortical convolutions. Cerebr. Cortex 15, 1900–1913.

Tzourio-Mazoyer, N., Landeau, B., Papathanassiou, D., Crivello, F., Etard, O., Delcroix, N., Mazoyer, B., Joliot, M., 2002. Automated anatomical labeling of activations in SPM using a macroscopic anatomical parcellation of the MNI MRI single-subject brain. Neuroimage 15, 273–289.

Uylings, H.B.M., Sanz-Arigita, E.J., de Vos, K., Pool, C.W., Evers, P., Rajkowska, G., 2010. 3D Cytoarchitectonic parcellation of human orbitofrontal cortex. Correlation with postmortem MRI. Psychiatr. Res. Neuroimaging 183, 1–20.

Welker, W., 1990. Why does cerebral cortex fissure and fold? A review of determinants of gyri and sulci. In: Jones, E., Peters, A. (Eds.), Cerebral Cortex, vol. 8b. Plenum Press, New York, USA, 3–136.

Xu, G., Knutsen, A.K., Dikranian, K., Kroenke, C.D., Bayly, P.V., Taber, L.A., 2010. Axons pull on the brain, but tension does not drive cortical folding. J. Biomech. Eng. 132, 071013.

Yang, F., Kruggel, F., 2008. Automatic segmentation of human brain sulci. Med. Image Anal. 12, 442–451.